

Temporal components of cholinergic terminal to dopaminergic terminal transmission in dorsal striatum slices of mice

Li Wang, Xiaoyu Zhang, Huadong Xu, Li Zhou, Ruiying Jiao, Wei Liu, Feipeng Zhu, Xinjiang Kang, Bin Liu, Sasa Teng, Qihui Wu, Mingli Li, Haiqiang Dou, Panli Zuo, Changhe Wang, Shirong Wang and Zhuan Zhou

State Key Laboratory of Biomembrane and Membrane Biotechnology and Beijing Key Laboratory of Cardiometabolic Molecular Medicine, Institute of Molecular Medicine and Peking-Tsinghua Center for Life Sciences and PKU-IDG/McGovern Institute for Brain Research, Peking University, Beijing, 100871, China

Key points

- The timing of synaptic transmission is critical to synaptic plasticity in the striatum.
- However, the timing of striatal dopamine (DA) release induced by cholinergic interneurons (ChIs) in the striatum is unclear.
- In this study, we focused on the temporal components of DA release and replenishment triggered by different pathways.
- We show that stimulation of ChIs induces DA release with a total delay of 20.6 ms, including 2.8 ms for action potential firing of ChIs, 7.0 ms for cholinergic transmission between acetylcholine terminals and DA terminals, and 10.8 ms for downstream DA release. The delay of DA release via this ChI pathway is 1.9 times that via the nigrostriatal pathways.
- We describe the time course of recovery of DA release via the two pathways and that of vesicle replenishment in DA terminals.
- Our work provides an example of unravelling the temporal building blocks during fundamental synaptic terminal–terminal transmission.

Abstract Striatal dopamine (DA) is critically involved in major brain functions such as motor control and deficits such as Parkinson's disease. DA is released following stimulation by two pathways: the nigrostriatal pathway and the cholinergic interneuron (ChI) pathway. The timing of synaptic transmission is critical in striatal circuits, because millisecond latency changes can reverse synaptic plasticity from long-term potentiation to long-term depression in a DA-dependent manner. Here, we determined the temporal components of ChI-driven DA release in striatal slices from optogenetic ChAT-ChR2-EYFP mice. After a light stimulus at room temperature, ChIs fired an action potential with a delay of 2.8 ms. The subsequent DA release mediated by nicotinic acetylcholine (ACh) receptors had a total latency of 17.8 ms, comprising 7.0 ms for cholinergic transmission and 10.8 ms for the downstream terminal DA release. Similar latencies of DA release were also found in striatal slices from wild-type mice. The latency of ChI-driven DA release was regulated by inhibiting the presynaptic vesicular ACh release. Moreover, we describe the time course of recovery of DA release *via* the two pathways and that of vesicle replenishment in

L. Wang and X. Zhang are contributed equally to this study.

DA terminals. Our work provides an example of unravelling the temporal building blocks during fundamental synaptic terminal–terminal transmission in motor regulation.

(Resubmitted 25 January 2013; accepted after revision 9 June 2014; first published online 27 June 2014)

Corresponding author Zhuan Zhou, Institute of Molecular Medicine, Peking University, 5 Yiheyuan Road, Beijing 100871, China. Email: zzhou@pku.edu.cn

Abbreviations ACh, acetylcholine; ACSF, artificial cerebrospinal fluid; AP, action potential; ARP, absolute refractory period; BSA, bovine serum albumin; CFE, carbon-fibre electrode; ChAT, choline acetyltransferase; ChI, cholinergic interneuron; DA, dopamine; EPSC, excitatory postsynaptic current; FCV, fast cyclic voltammetry; LTD, long-term depression; LTP, long-term potentiation; nAChR, nicotinic acetylcholine receptor; PPR, paired pulse ratio; SNc, substantia nigra pars compacta; STDP, spike-timing-dependent plasticity; VACHT, vesicular ACh transporter.

Introduction

Dopamine (DA) is essential in determining the brain states of mental health and is involved in diseases such as depression, drug addiction and Parkinson disease (Kandel *et al.* 2000). Most DA neurons are located in the midbrain and project axons to the distant striatum. The action potential (AP) firing of midbrain DA neurons propagates along the medial forebrain bundle *via* the ascending nigrostriatal pathway, and evokes DA release in the striatum (Nicola *et al.* 2000). Cholinergic activity is reported to regulate dopaminergic transmission (Zhou *et al.* 2001; Rice & Cragg, 2004; Zhang & Sulzer, 2004). Using fast cyclic voltammetry (FCV) for DA recording, it was recently reported that the activity of cholinergic interneurons (ChIs), terminals of which target on the DA terminals, drive DA release independent of ascending activity from the nigrostriatal pathway (Cachope *et al.* 2012; Threlfell *et al.* 2012). The ChI pathway comprises a complex structure of synaptic terminal–terminal connection which triggers cholinergic transmission-induced dopaminergic transmission. Generally, there are three types of synapses in neuronal circuits (axo-somatic type I, axo-dendritic type II and axo-axonic type III). Type I and II synapses have one axon terminal, while type III synapses have one pre-synaptic axon terminal on another axon terminal (Kandel *et al.* 2000). Type I and II synapses have been intensively studied, while little is known about the properties of the type III synapse, because it is technically difficult to selectively stimulate one of the two axonal terminals within the synapse. In the striatum, ultrastructural evidence suggests that the cholinergic interneuron forms axo-axonic contacts (Descarries *et al.* 1997). This cholinergic transmission could be ‘wiring transmission’ *via* classical specialized synaptic contacts (Wainer *et al.* 1984; Phelps *et al.* 1985) or ‘volume transmission’ *via* either activating extrasynaptic nicotinic acetylcholine receptors (nAChRs) by acetylcholine (ACh) spillover from the synaptic cleft or diffusion from asynaptic axonal varicosities (Descarries & Mechawar, 2000; Dani & Bertrand, 2007). In either case, the cholinergic axo-axonic

contacts may be considered functionally equal to the type III synapse in transmitting signal.

The timing of synaptic transmission is critical to determine whether long-term potentiation (LTP) or long-term depression (LTD) forms in a synapse (Markram *et al.* 1997; Dan & Poo, 2006). The total latency of synaptic transmission includes the temporal components of AP propagation to the presynaptic terminal, Ca²⁺ influx, transmitter release, transmitter diffusion across the synaptic cleft and generation of postsynaptic current (Augustine *et al.* 1987; Sabatini & Regehr, 1999). At room temperature, the latency of cholinergic synaptic transmission at the neuromuscular junction is ~1 ms in frog (Katz & Miledi, 1965), while glutamatergic synaptic transmission requires ~1 ms in squid axon (Augustine *et al.* 1985), and 1–5 ms in the rodent locus coeruleus (Huang *et al.* 2007) and cerebellum (Sabatini & Regehr, 1996). In striatal DA terminals, however, the temporal components of ChI-driven DA release remain unknown, because the temporal resolution of FCV (100 ms) is too low (Cachope *et al.* 2012; Threlfell *et al.* 2012).

Neurotransmission includes neurotransmitter release from presynaptic vesicles. Vesicles can be grouped into different vesicle pools according to such factors as their Ca²⁺ dependence, release latency, release probability and replenishment rate. It is well known that different vesicle pools exist even in a single adrenal chromaffin cell or pre-synaptic terminal (Sorensen *et al.* 2003; Rizzoli & Betz, 2005; Neher & Sakaba, 2008; Liu *et al.* 2011; Zhang *et al.* 2011). After presynaptic vesicular release, the vesicle pool must be replenished within seconds or minutes to support the next run of synaptic transmission (for reviews see Sudhof, 2004; Wu, 2004; Rizzoli & Betz, 2005). Given the importance of the timing of dopaminergic transmission in its postsynaptic effects (Arbuthnott & Wickens, 2007) and behaviours, such as cue detection, movement and reward (Schultz, 2007), it is critical to determine the timing of striatal DA release *via* different pathways, as well as the replenishment of vesicle pools after depletion induced by the preceding release. Part of the present study has been submitted in abstract form (Wang *et al.* 2013).

Methods

Animals

ChAT-ChR2-EYFP transgenic mice (Ren *et al.* 2011; Zhao *et al.* 2011) and wild-type C57BL/6 mice of either sex were used following a protocol approved by the Peking University Animal Use and Care Committee. Electrochemical recording was performed in slices from mice 3–10 weeks old, patch-clamp recording was performed in slices from mice 3–4 weeks old and immunofluorescence staining was performed in slices from adult mice.

Acute brain slices

Brain slices were prepared as previously described (Huang *et al.* 2007; Zhao *et al.* 2011; Zhang *et al.* 2012). After anaesthesia by injection of chloral hydrate (350 mg kg⁻¹, i.p.) as previously described (Liu *et al.* 2011), mice were transcardially perfused with 5–10 ml ice-cold dissection solution of the following composition (in mM): 92 *N*-methyl-D-glucamine, 2.5 KCl, 0.5 CaCl₂, 10 MgSO₄, 1.2 NaH₂PO₄, 30 NaHCO₃, 25 glucose, 20 Hepes, 5 (L)-ascorbic acid and 3 sodium pyruvate (adjusted to pH 7.3–7.4 with concentrated HCl) (saturated with 95% O₂ and 5% CO₂). Mice were then decapitated and the brain removed into the dissection solution. Horizontal striatal or coronal midbrain slices (300 μm) were prepared with a vibratome (VT1200s, Leica Microsystems AG, Wetzlar, Germany) in ice-cold dissection solution. Slices were allowed to recover for 10–15 min at 33°C in dissection solution and incubated thereafter for at least 1 h at room temperature in artificial cerebrospinal fluid (ACSF) of the following composition (in mM): 112 NaCl, 2.5 KCl, 2 CaCl₂, 2 MgSO₄, 1.2 NaH₂PO₄, 30 NaHCO₃, 12.5 glucose, and 20 Hepes (saturated with 95% O₂ and 5% CO₂). The ACSF was supplemented with 5 mM (L)-ascorbic acid, 3 mM sodium pyruvate, 100 units ml⁻¹ penicillin G sodium and 100 μg ml⁻¹ streptomycin sulfate. Slices were superfused (1–2 ml min⁻¹) with ACSF (without the supplements) at room temperature during electrophysiological experiments. All chemicals were from Sigma-Aldrich (St Louis, MO, USA) except when specified otherwise.

Electrophysiological recordings

Whole-cell patch-clamp recordings were performed at room temperature (22–25°C), using an EPC9/2 amplifier (HEKA Elektronik, Lambrecht/Pfalz, Germany) as described (Chen *et al.* 2005; Huang *et al.* 2007). The resistances of patch pipettes were 3–4 MΩ. Intracellular recording solution contained (in mM): 130 potassium gluconate, 5 KCl, 4 MgCl₂, 10 Hepes, 10 Na₂-phosphocreatine, 0.2 EGTA, 2 Mg-ATP and 0.4

Na₃-GTP (adjusted to pH 7.2 with KOH). Whole-cell recordings were obtained under differential interference contrast visual control with a BX51WI microscope (Olympus, Tokyo, Japan). To keep the ChIs silent, a small hyperpolarizing current (–200 pA) was injected in the current-clamp experiments. Signals were low-pass filtered at 2.9 kHz and digitized at 20 kHz. The liquid junction potential was not corrected. A drug-puffing device (MPS1, Yibo Instruments Inc., Wuhan, China) with a fast exchange time (<100 ms) among eight channels was used to deliver drugs to the recording site.

Electrochemical recordings

Standard carbon-fibre electrodes (ProCFEs, Dagan Instruments, Minneapolis, MN, USA) were used to detect DA as described previously (Huang *et al.* 2007; Wang *et al.* 2011) with some modifications of insulation (glass), carbon-fibre size (7 μm in diameter) and sensor length. The exposed tip (200–300 μm in length) was inserted into the subsurface of the striatal slice (laterodorsal striatum). Voltammetry was performed with a triangular waveform (–0.4 to 1.0 V vs. Ag/AgCl, 300 V s⁻¹) at 16 Hz. The electrode was held at –0.4 V between scans. The output signal was low-pass filtered at 2.9 kHz and digitized at 20 kHz. Amperometry was performed at a holding potential of 780 mV. The amperometric current (*I*_{amp}) output signal was low-pass filtered at 100 Hz and digitized at 2 kHz. The electrochemical experiments were performed at room temperature, except for that shown in Fig. 3*H* and *I*, which were performed at 17–32°C.

Optogenetic stimulation

A 470 nm light-emitting diode (Yibo Instruments) was used for optogenetic stimulation following standard procedures (Boyden *et al.* 2005). The output light was coupled to the microscope and focused onto the tissue by a 60× water-immersion objective lens. The diameter of the light stimulus spot was 440 μm and the maximal light intensity reaching the tissue was ~4.2 mW mm⁻². The stimulation time of light pulses was controlled by a 5 V TTL signal from the EPC9/2 amplifier.

Electrical stimulation

Bipolar platinum electrodes (150 μm in diameter) with a tip separation of 20 μm were used for local electrical field stimulation. For electrochemical experiments, both the stimulating electrode and carbon-fibre electrodes (CFEs) were placed parallel at 100 μm separation in the horizontal laterodorsal striatum slices. For patch-clamp recording of AP firing in DA neurons, both the stimulating electrode and the patch pipette were placed parallel at 100 μm

separation in the coronal substantia nigra pars compacta (SNc) slices. Field pulses (0.2 ms, 0.3–1.4 mA) generated by a stimulator with an isolation unit (S88K, Grass Instruments, Warwick, RI, USA) were used to induce DA release or AP firing. The stimulation time of field pulses was controlled by a 5 V TTL signal from the EPC9/2 amplifier.

Immunohistochemistry

Immunostaining was performed as previously described (Huang *et al.* 2007). Briefly, adult mice were anaesthetized and transcardially perfused with normal saline followed by 4% paraformaldehyde. Brains were dissected, post-fixed overnight in 4% paraformaldehyde, cryoprotected in 30% sucrose and frozen in tissue-freezing medium (Tissue-Tek). The slices were sectioned at 50 μm on a cryostat and floated in PBS. Sections were rinsed with 0.2% Triton X-100 in PBS for 30 min, and then blocked with 2% bovine serum albumin (BSA) in PBS for 1 h at room temperature. Sections were then incubated with primary antibodies in BSA at 4°C overnight. The primary antibodies were: goat anti-ChAT (1:500, EMD Millipore, Billerica, MA). Sections were rinsed and incubated for 3 h at room temperature with the second antibodies Alexa546-conjugated donkey anti-goat (1:500, Life Technologies Inc., Carlsbad, CA, USA), rinsed again, stained with 1 μM DAPI (Life Technologies) and mounted on slides with mounting solution (Dako, Glostrup, Denmark). Immunofluorescence-labelled sections were imaged under a confocal laser scanning microscope (Zeiss LSM 700, Carl Zeiss, Göttingen, Germany).

Theory of replenishment components within terminal-terminal transmission

Synaptic transmission between the axons of two neurons is mediated by an axo-axonic synapse (type III terminal-terminal structure), which consists of axon terminal A (presynapse of cell A) on another axon terminal B (presynapse of cell B, also postsynaptic to cell A). Following depletion of the vesicle pool by the first of a pair of stimuli, the recovery of terminal-terminal synaptic transmission can be tested by the second stimulus. For dopaminergic transmission in the striatum, paired stimuli with a short interpulse interval cause a dramatic depression of DA release (Schmitz *et al.* 2002; Cragg, 2003; Zhang & Sulzer, 2004).

Paired-pulse ratio (PPR) is commonly used to study recovery of release in chromaffin cells, glutamate synapses and dopaminergic terminals (Cragg, 2003; Zhang & Sulzer, 2004; Neher & Sakaba, 2008; Zhang *et al.* 2011). There are several hypotheses to interpret the recovery of vesicle release, including Ca^{2+} -dependent release

probability (Rice & Cragg, 2004), G protein-coupled receptor-mediated auto-inhibition (Schmitz *et al.* 2002) and vesicle pool replenishment (Neher & Sakaba, 2008; Zhang *et al.* 2011). To quantitatively interpret our PPR results, we use the vesicle pool hypothesis. $Sa(t)$ and $Sb(t)$ are defined as transmitter release of terminals A and B, respectively. The activation of terminal A induces the final transmitter release signal from terminal B ($S(t)$):

$$S(t) = \begin{cases} 0, & (t < T_{\text{ARP}}) \\ Sb'(t), & (t \geq T_{\text{ARP}}) \end{cases} \quad (1)$$

where $S(t)$ is the transmitter release signal from terminal B that was triggered by the activation of terminal A. $S(t)$ (but not $Sa(t)$ or $Sb(t)$) can be directly detected. T_{ARP} is the refractory time during which $Sa(t)$ is a sub-threshold input to induce AP firing or transmitter release at terminal B, which is determined by both replenishment of the vesicle pool in terminal A and nAChR-induced DA release in terminal B. The ChI-driven DA release signal pathway consists of terminal A release, nAChR activation and terminal B release. Each of terminals A and B processes gradual vesicle release, while their linker, nAChR-induced DA release, behaves as a ‘step-like component’ in eqn (1). The strength of the input to terminal B is determined not only by terminal A but also by nAChRs on terminal B. Thus, although $S(t)$ is vesicle release from terminal B, $S(t) = Sb'(t) \neq Sb(t)$ even for $t \geq T_{\text{ARP}}$, unless the cholinergic transmission and nAChRs are fully recovered within T_{ARP} .

Regarding the individual terminals A and B, we assume (1) every stimulus triggers the same Ca^{2+} signal, and (2) the replenishment of vesicle pools in terminals A and B consists of components of the established $1 - e^{-\frac{t}{\tau}}$ format (termed the ‘classical component’ (Otsuka *et al.* 1962; Elmqvist & Quastel, 1965; Katz, 1969; Dittman & Regehr, 1998; Neher & Sakaba, 2008; Pan & Zucker, 2009)). Assuming terminals A and B contain only a single component, we have:

$$Sa(t) = A(1 - e^{-\frac{t}{\tau_a}}) \quad (2)$$

$$Sb(t) = B(1 - e^{-\frac{t}{\tau_b}}) \quad (3)$$

Equation (2) (or eqn (3)) describes the ‘classical law’ of vesicle pool replenishment for a single synaptic terminal. Note, for simplicity, that we further assume the replenishment (measured by the release signal following the second stimulus) in eqns (1)–(3) to be $S = Sa = Sb = 0$ immediately after stimulation ($t = 0$), or the vesicle pools are assumed to be fully depleted by the AP induced by the first of the paired stimuli. More generally, if the depletion level of a vesicle pool is α ($0 \leq \alpha \leq 1$), such as the pool in eqn (2), the vesicle pool component has the general form

$A(1 - \alpha^* e^{-\frac{1}{\tau a}})$. Note the assumptions upon using eqns (1)–(3).

Data analysis

Pulse v8.80 software (HEKA Elektronik) was used for data acquisition in both patch-clamp and amperometry experiments. Patchmaster v2.20 software (HEKA Elektronik) was used for acquisition of FCV data. Igor Pro 6.22 software (Wavemetrics, Lake Oswego, OR, USA) was used to analyse the patch-clamp, amperometry and FCV data. Stimulation (Estim and Lstim)-induced transient artifacts in the amperometric traces were removed for clarity. The latency of DA release signals/AP events was defined by the interval between stimulus onset and time at 50% response. Data are presented as mean \pm standard error of the mean (SEM). Statistical differences between two groups were evaluated with Student's *t* test. $P < 0.05$ was considered statistically significant.

Results

Selective excitation of cholinergic interneurons triggered DA release from striatum

We used ChAT-ChR2-EYFP transgenic mice to selectively stimulate ChIs in horizontal striatal slices. Immunofluorescence staining showed that ChR2-EYFP was strongly and specifically expressed in both the somata and processes of ChIs in the dorsal striatum. The interneurons were identified by the expression of choline acetyltransferase (ChAT, Fig. 1A). ChR2-EYFP was not expressed in DA neurons identified by an antibody against tyrosine hydroxylase in either the striatum or the ventral midbrain (data not shown).

To determine whether a light stimulus (Lstim) selectively and effectively excited ChIs, we performed whole-cell patch-clamp measurements. A standard blue light pulse at 470 nm, 1 ms in duration, rapidly and reproducibly elicited a single AP under current-clamp and a fast inward current under voltage-clamp in ChIs in the dorsal striatum (Fig. 1B). Repetitive patterned Lstim pulses (5–20 Hz) evoked trains of APs (data not shown). This Lstim-induced AP firing was sensitive to tetrodotoxin (data not shown). By contrast, no APs were elicited in DA neurons in the SNc or the ventral tegmental area (VTA, data not shown), indicating that Lstim selectively stimulated ChIs in the dorsal striatum but not DA neurons in the midbrain.

We used both electrochemical FCV and amperometry to assess DA release in the laterodorsal striatum. Immediately after a single Lstim, an abrupt increase of extracellular DA overflow was detected by standard FCV with a micro-CFE

(sampling rate ≤ 16 Hz, Fig. 1C). After subtracting the background current in the cyclic voltammograms, an oxidative peak (+650 mV) and a reductive peak (–200 mV) were detected in the striatal slice; these were identical to the FCV of 10 μM DA applied *in vitro*, indicating that DA release was responsible for the Lstim-induced electrochemical signal (Fig. 1C). To achieve higher temporal resolution, we changed the recording mode from FCV to amperometry with the CFE at a constant holding potential of +780 mV. We used a 2 kHz sampling rate, which is >100 times higher than that by FCV, to record DA release as amperometric current (I_{amp}). Lstim-induced I_{amp} (Lstim) represented ChI-driven DA release ($I_{\text{amp}}(\text{ChID}) = I_{\text{amp}}(\text{Lstim})$, Fig. 1D and E). The relationship between $I_{\text{amp}}(\text{Lstim})$ and light intensity was fitted with a Hill function (see Fig. 3F) and the profile of $I_{\text{amp}}(\text{Lstim})$ was similar to the DA release induced by a conventional local electrical stimulus (Estim) ($I_{\text{amp}}(\text{Estim})$, Fig. 1D and E). Due to the low temporal resolution of FCV (sampling interval ≥ 62 ms), the precise onset timing of the evoked DA release could not be accurately measured, while the I_{amp} signal provided the necessary resolution to investigate the millisecond timing information of the striatal DA release (Fig. 1C–E; see also Phillips *et al.* 2003).

Timing of cholinergic transmission-induced DA release

In contrast to the DA release induced by Lstim that selectively activated the ChI pathway, local Estim activated both the ChI pathway (activation of ChIs or their axons) and the nigrostriatal pathway (activation of DA axons in the striatum), and induced a mixed DA release with a biphasic onset shown in $I_{\text{amp}}(\text{Estim})$ (Figs 1E and 2A and B; see Wang *et al.* 2013). The phase I component represented DA release *via* the ascending nigrostriatal pathway, while phase II represented DA release *via* the ChI pathway, because a specific antagonist of $\beta 2$ -containing nAChRs, DH β E, blocked only the phase II but not the phase I component of $I_{\text{amp}}(\text{Estim})$ (Fig. 2B). This is consistent with previous studies showing that DH β E abolishes the ChI-driven DA release induced by Lstim (Cachope *et al.* 2012; Threlfell *et al.* 2012). In addition, the latency of phase II of $I_{\text{amp}}(\text{Estim})$ was equal to the latency of $I_{\text{amp}}(\text{Lstim})$ (Fig. 2B), which also confirmed the dual pathway origin of the biphasic onset of $I_{\text{amp}}(\text{Estim})$.

Next, we investigated the temporal components during the initiation of ChI-driven DA release. We recorded the APs with whole-cell patch-clamp and the DA release signals with amperometry in the laterodorsal striatum in horizontal striatal slices. Following Lstim, the latency of APs in ChIs (t_{CAP}) was 2.8 ± 0.1 ms (as measured at the somata of ChIs in dorsal striatum slices), the

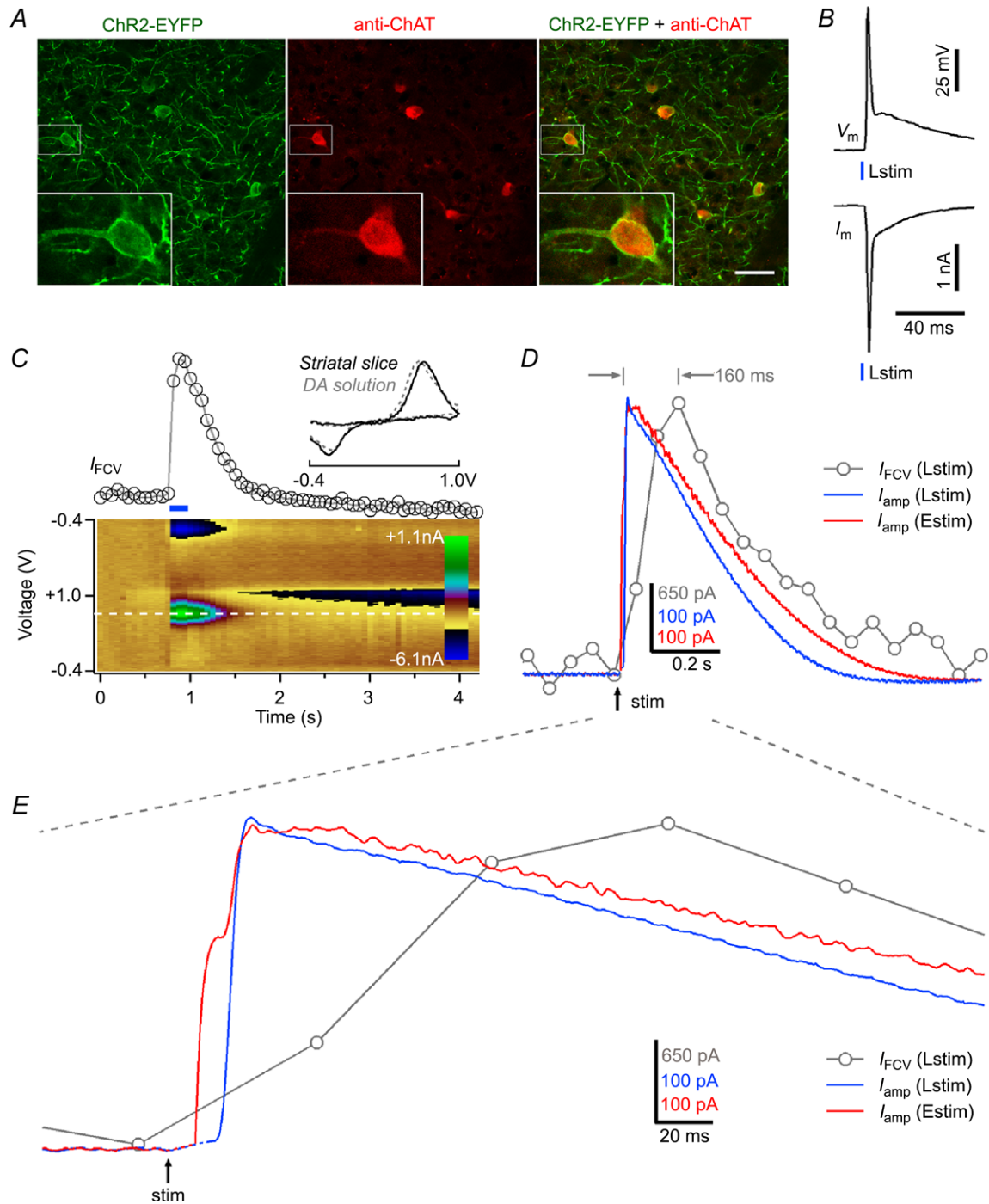


Figure 1. Optogenetic stimulation induces DA release triggered by cholinergic transmission in the striatum

A, ChR2-EYFP (green) was strongly and selectively expressed in cholinergic interneurons (ChIs) (labelled with anti-ChAT, red) in the dorsal striatum of ChAT-ChR2-EYFP mice. Scale bar: 50 μm . **B**, A transient light stimulus (470 nm, 1 ms) immediately triggered a single AP (V_m , recorded under current-clamp, $n = 11$) and a fast inward current (I_m , recorded under voltage-clamp, $n = 12$) in a ChI. **C**, representative FCV trace of Lstim-induced DA release via the ChI pathway ($n = 9$). *Upper*, FCV-derived I_{FCV} -time plot. I_{FCV} is the peak oxidative current at 665 mV; *lower*, I - V - t pseudocolour plot (Phillips *et al.* 2003) with time corresponding to the upper I_{FCV} . Lstim was applied for 200 ms. *Inset*, normalized background-subtracted FCV voltammograms of DA release in the striatal slice (continuous line) vs. in 10 μM DA *in vitro* (dashed line). **D**, representative amperometric traces of DA release induced by a light stimulus (I_{amp} (Lstim), $n = 25$) or an electrical stimulus (Estim, I_{amp} (Estim), $n = 19$) vs. the I_{FCV} -time trace of DA release induced by Lstim (FCV(Lstim), $n = 9$). **E**, expanded view of the traces shown in **D**.

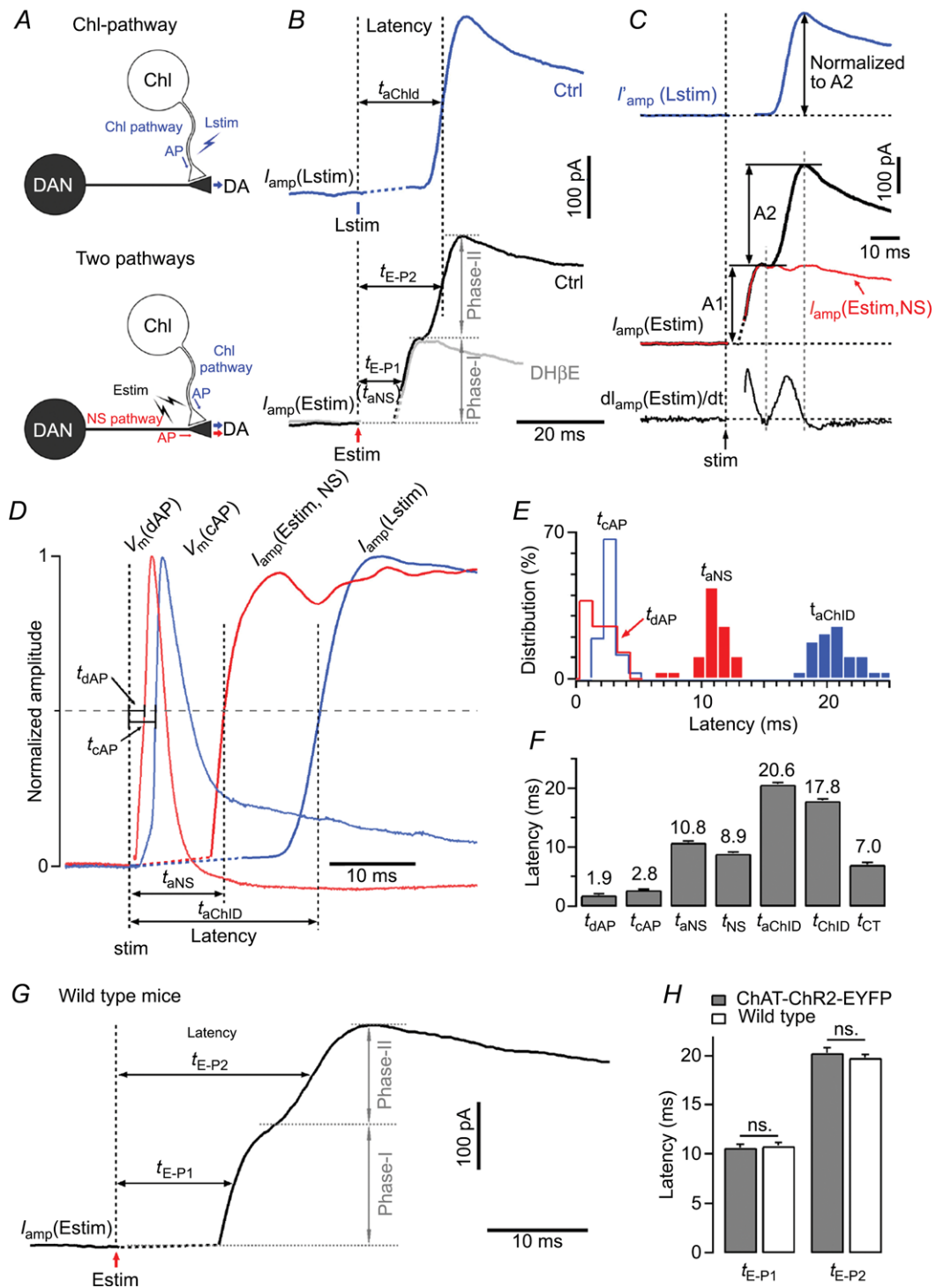


Figure 2. Timing of presynaptic and postsynaptic signals during cholinergic interneuron-driven DA release

A, schema of Lstim-induced DA release via the Chl pathway and Estim-induced DA release via both the nigrostriatal (NS) and Chl pathways. Chl, cholinergic interneuron; DAN, DA neuron. B, Lstim-induced DA release ($I_{amp}(Lstim)$) showed a monophasic onset ($n = 25$), while Estim-induced DA release ($I_{amp}(Estim)$) showed a biphasic onset ($n = 19$). $I_{amp}(Estim) = I_{amp}(Estim, NS) + I_{amp}(Estim, ChID)$. $I_{amp}(Estim, NS)$ and $I_{amp}(Estim, ChID)$ corresponded to the nigrostriatal DA release component (phase I) and the Chl-driven DA release component (phase II), respectively. The total latency of DA release was determined by the interval between stimulus onset and time at 50% response. The latency (t_{E-P2}) of $I_{amp}(Estim, ChID)$ and the latency (t_{aChID}) of $I_{amp}(Lstim)$ were nearly identical, both of

total latency of $I_{\text{amp}}(\text{Lstim})$ via the ChI pathway (t_{aChID} , 'aChID' denotes AP + ChI-driven DA release (ChID)) was 20.6 ± 0.3 ms, and the ChID latency from cholinergic AP firing to DA release ($t_{\text{ChID}} = t_{\text{aChID}} - t_{\text{cAP}}$) was 17.8 ± 0.3 ms (Fig. 2E and F). Following Estim, the latency of APs in DA neurons (t_{dAP}) was 1.9 ± 0.2 ms (as measured at the somata of DA neurons in SNc slices). To calculate the total latency of $I_{\text{amp}}(\text{Estim, NS})$ via the nigrostriatal pathway (t_{aNS}), phase I of $I_{\text{amp}}(\text{Estim})$ was mathematically isolated as shown in Fig. 2C. The t_{aNS} was 10.8 ± 0.2 ms, and the latency of nigrostriatal DA release (t_{NS} , from dopaminergic AP firing to release) was 8.9 ± 0.2 ms (Fig. 2D–F). Notably, there was a gap of 7.0 ± 0.4 ms between t_{ChID} and t_{aNS} . Since terminal DA release is initiated after the preceding cholinergic transmission has been accomplished, the 7.0 ms gap between t_{ChID} and t_{aNS} should represent the latency of cholinergic transmission in the ChI pathway ($t_{\text{CT}} = t_{\text{ChID}} - t_{\text{aNS}} = t_{\text{aChID}} - t_{\text{aNS}} - t_{\text{cAP}}$, 'CT' denotes cholinergic transmission). In addition to factors downstream of Ca^{2+} , the latency between a cholinergic excitatory postsynaptic current (EPSC) and DA release also depends on whether the EPSC induces an AP in the DA terminal. Note, in the DA terminal of ChI-driven DA release in Fig. 2B, we considered that the phase I DA signal was produced by the Estim-induced first AP via the nigrostriatal pathway. However, whether the phase II DA signal via the ChI pathway was triggered by the fractional Ca^{2+} influx through nAChRs (Zhou & Neher, 1993) with (as assumed in Fig. 2B) or without the second AP remained unknown. t_{CT} would be slightly longer (extended for $<t_{\text{aAP}}$) if the Estim-induced cholinergic EPSC did not trigger the second AP for the phase II DA signal in Fig. 2B.

In addition to ChAT-ChR2-EYFP transgenic mice, we also recorded the Estim-induced DA release from dorsal striatum slices in wild-type C57BL/6 mice. The biphasic onset of $I_{\text{amp}}(\text{Estim})$ was also found in these mice (Fig. 2G). The latencies of DA release via the two pathways were nearly identical in the wild-type and

transgenic mice (Fig. 2H). Thus, overexpression of the vesicular ACh transporter (VACHT) in ChAT-ChR2-EYFP mice did not affect the timing of DA release in brain slices, although some behaviours are changed in wild-type versus ChAT-ChR2-EYFP mice (Kolisyk *et al.* 2013). Regarding temperature dependence, $I_{\text{amp}}(\text{Lstim})$ latencies were 46.9 ± 2.3 ms at 17°C , 21.3 ± 0.8 ms at 25°C and 15.5 ± 1.0 ms at 32°C , indicating that ChI-driven DA release was accelerated at higher temperature (32°C) (Fig. 3H and I).

Regulation of the latency of ChI-driven DA release by cholinergic presynaptic mechanisms

To investigate the mechanism of how cholinergic transmission affects the latency of ChI-driven DA release, we examined the effects on latency of depleting the cholinergic vesicle pool. Vesamicol, an inhibitor of the VACHT (Enomoto, 1988; Lupa, 1988), inhibits Estim-induced DA release (Zhou *et al.* 2001), suggesting that endogenous ACh has a regulatory effect on DA release. Lstim-induced DA release gradually declined to $3.0 \pm 0.9\%$ of control after puffing $30 \mu\text{M}$ vesamicol from 2 to 16 min, and recovered to $64 \pm 14\%$ after 2 h washout (Fig. 3A and B), suggesting that the ChI pathway DA release is mediated by vesicular ACh release. Meanwhile, the normalized amperometric recordings showed that the latency of $I_{\text{amp}}(\text{Lstim})$ was extended from 20.7 ± 0.5 to 24.9 ± 0.7 ms after vesamicol treatment (Fig. 3C), and recovered to 22.7 ± 0.7 ms after washout. The increase in latency was in parallel with the reduction of the amplitude during the application of vesamicol (Fig. 3D), suggesting that the latency is dependent on the amount of ACh released from pre-synaptic terminals. We also tested the correlation of latency and amplitude of $I_{\text{amp}}(\text{Lstim})$ by varying the intensity of light stimulation. Both the latency and the amplitude of $I_{\text{amp}}(\text{Lstim})$ were dependent on the intensity of Lstim (Fig. 3E). Similar to the data shown in Fig. 3D, the

which were longer than the latency ($t_{\text{E-P2}}$ or t_{aNS}) of $I_{\text{amp}}(\text{Estim, NS})$. DH β E ($1 \mu\text{M}$), a specific antagonist of β 2-containing nAChRs, selectively blocked the phase II but not the phase I component of $I_{\text{amp}}(\text{Estim})$ ($n = 4$). C, the typical Estim-induced biphasic DA release signal $I_{\text{amp}}(\text{Estim})$ contained a phase I component (amplitude A1, $I_{\text{amp}}(\text{Estim, NS})$) and a phase II component (amplitude A2, $I_{\text{amp}}(\text{Estim, ChID})$). The pure nigrostriatal component of Estim-induced DA release (phase I, $I_{\text{amp}}(\text{Estim, NS})$) was mathematically isolated by subtracting $I_{\text{amp}}(\text{Estim, ChID})$ from total $I_{\text{amp}}(\text{Estim})$: $I_{\text{amp}}(\text{Estim, NS}) = I_{\text{amp}}(\text{Estim}) - I_{\text{amp}}(\text{Estim, ChID})$. $I_{\text{amp}}(\text{Estim, ChID})$ was estimated by direct measurement of Lstim-induced $I_{\text{amp}}(\text{Lstim})$: $I_{\text{amp}}(\text{Estim, ChID}) = I_{\text{amp}}(\text{Lstim}) \times (\text{A2}/\text{amplitude of } I_{\text{amp}}(\text{Lstim}))$. D, latencies of APs in a DA neuron (t_{dAP}), a ChI (t_{cAP}), and the total latencies of nigrostriatal (t_{aNS}) and ChI-driven DA releases (t_{aChID}). The latency t_{aNS} was obtained from the mathematically isolated traces of nigrostriatal DA release ($I_{\text{amp}}(\text{Estim, NS})$). E, distribution of observed t_{dAP} , t_{cAP} , t_{aNS} and t_{aChID} . F, from the same data as in D, summary of the latencies of AP firing in DA neurons (t_{dAP} , $n = 16$), ChIs (t_{cAP} , $n = 36$), total latency of nigrostriatal DA release (t_{aNS} , $n = 27$), latency of nigrostriatal DA release after AP firing ($t_{\text{NS}} = t_{\text{aNS}} - t_{\text{dAP}}$), total latency of ChI-driven DA release (t_{aChID} , $n = 27$) and latency of ChI-driven DA release after AP firing ($t_{\text{ChID}} = t_{\text{aChID}} - t_{\text{cAP}}$), as well as the difference between t_{ChID} and t_{aNS} ($t_{\text{CT}} = t_{\text{aChID}} - t_{\text{aNS}} - t_{\text{cAP}}$, $n = 18$). G, representative amperometric trace of Estim-induced DA release ($I_{\text{amp}}(\text{Estim})$) in a striatal slice from a wild-type C57BL/6 mouse. $t_{\text{E-P1}}$, latency of phase I of $I_{\text{amp}}(\text{Estim})$; $t_{\text{E-P2}}$, latency of phase II of $I_{\text{amp}}(\text{Estim})$. H, summary of the latency of $I_{\text{amp}}(\text{Estim})$ in ChAT-ChR2-EYFP mice ($n = 16$) vs. wild-type C57BL/6 mice (unpaired t test, $n = 13$).

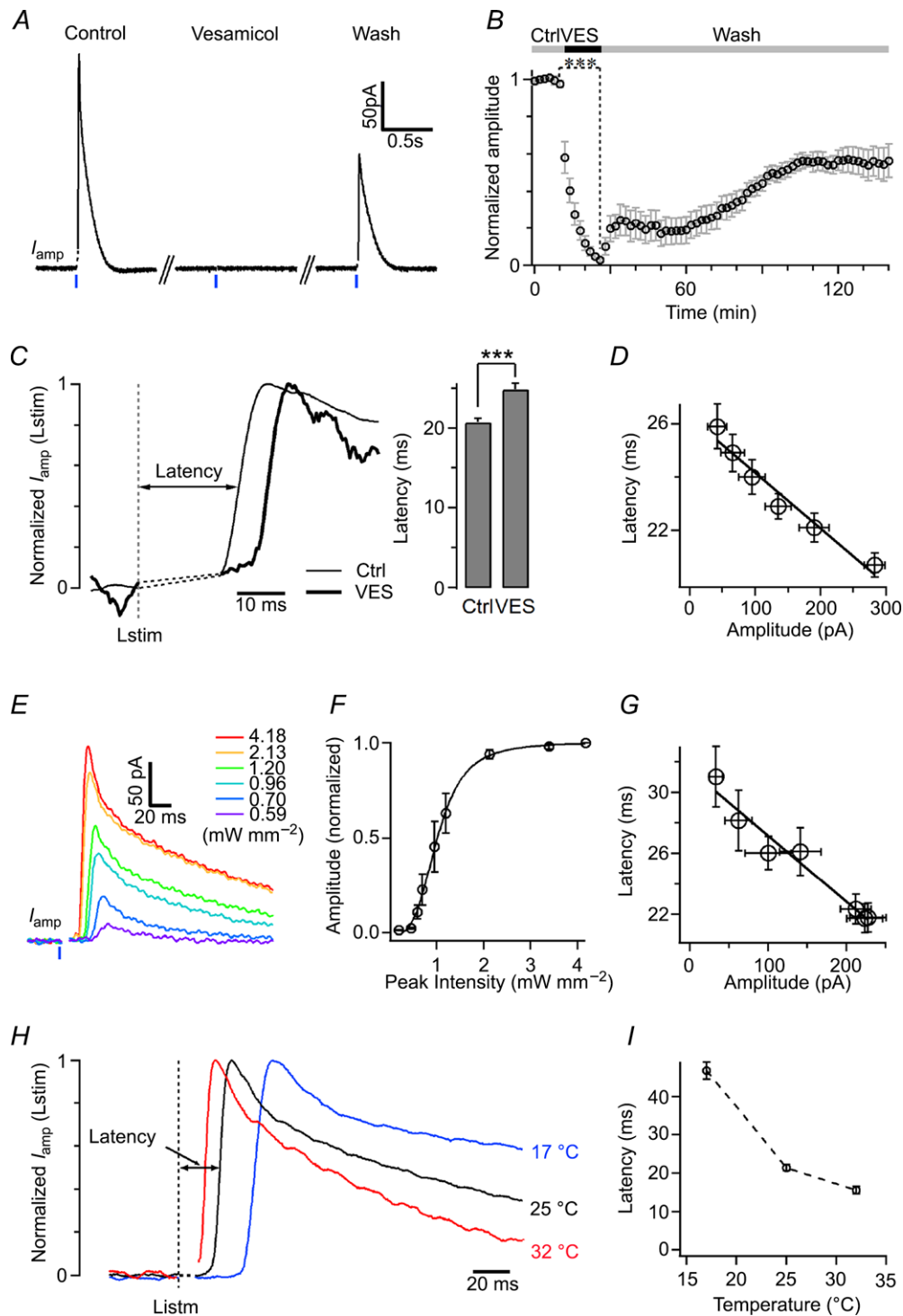


Figure 3. Regulation of the latency of cholinergic interneuron-driven DA release by presynaptic cholinergic transmission, stimulation intensity and temperature

A, depletion of vesicular ACh by 30 μM vesamicol (VES, an inhibitor of the vesicular ACh transporter) greatly reduced the amplitude of Lstim-induced DA release to 3.0 ± 0.9% of control (paired *t* test, *P* < 0.001, *n* = 7). *B*, time course of the effect of VES on the amplitude of DA release. *C*, application of VES for 8 min reversibly prolonged the latency of Lstim-induced DA release from 20.7 ± 0.5 ms in control to 24.9 ± 0.7 ms with VES (paired *t* test, *P* < 0.001, *n* = 6). *I*_{amp}(Lstim) traces were normalized for latency determination. *D*, the latency was in inverse proportion to the amplitude ($y = -20.8x + 26.2$, where *y* is the latency in ms, and *x* is the amplitude in pA, *R*² = 0.957). *E*, representative traces of DA release induced by Lstim at different intensities (*n* = 7). *F*,

correlation between latency and amplitude was fitted by a linear function (Fig. 3G). Thus, presynaptic ACh release concurrently regulates the quantity and the timing of subsequent DA release.

Replenishment of the dopaminergic vesicle pool

In a single terminal synapse, transmission requires replenishment of the presynaptic vesicle pool. In the complex synapse of ChI-driven DA release, a recovery period is required to recruit the depleted presynaptic vesicle pools in the two cascade terminals (i.e. ACh and DA pools) before it is ready to reproduce the same level of DA release as the previous one. Next, we examined the recovery of the ChI pathway after stimulation.

The recovery rate of the DA release was determined with PPR tests (Betz, 1970; Kusano & Landau, 1975; Schmitz *et al.* 2002). We applied paired Lstim for the recovery rate (PPR_{Lstim}) of ChI-driven DA release, and paired Estim for the recovery rate (PPR_{Estim}) of the mixed (nigrostriatal and ChI-driven) DA release (Fig. 4A and B). The $I_{amp}(Lstim)$ evoked by the second pulse at a 1 s interval in paired Lstim was almost completely suppressed ($PPR_{Lstim} = 2.0 \pm 0.5\%$), while the $I_{amp}(Estim)$ evoked by the second pulse in paired Estim at a 1 s interval recovered to $9.2 \pm 1.2\%$ ($PPR_{Estim} = 9.2 \pm 1.2\%$). Both $I_{amp}(Lstim)$ and $I_{amp}(Estim)$ fully recovered ($PPR_{Lstim} = PPR_{Estim} = 100\%$) within 120 s after the first pulse. PPR_{Lstim} and PPR_{Estim} are plotted in Fig. 4B. A notable difference between the recovery rates of PPR_{Lstim} and PPR_{Estim} was that within the initial 1 s after the first pulse, the PPR_{Lstim} was in an absolute refractory period (ARP, time period when $PPR_{Lstim} < 2\%$), but PPR_{Estim} partially remained (Fig. 4B). After the ARP ($T_{ARP} = 1$ s), the PPR_{Lstim} recovered following a single exponential function with $\tau_{ChID} = 21$ s (Fig. 4B). This result differs from a previous finding that ARP is absent in the nucleus accumbens, although the PPR (100 s) is $\sim 85\%$ (Cachope *et al.* 2012), which is similar to that in the dorsal striatum (Fig. 4B). In addition, as reported before (Threlfell *et al.* 2012), we confirmed that neither D₂ receptors nor mAChRs are responsible for the ARP (data not shown).

To determine whether the suppression of ChI-driven DA release is caused by full depletion of the dopaminergic

vesicle pool or by a failure of cholinergic transmission, and to further investigate the time course of dopaminergic pool replenishment following Lstim, we designed a protocol with mixed Lstim and Estim. Lstim at 5 Hz was applied to continually deplete the cholinergic transmission. During the refractory period from the second to the last pulse of the 5 Hz Lstim, DA release could not be induced by Lstim but was induced by Estim (Fig. 4C). This Estim-induced DA release during the ARP could be either from the remaining/recycled dopaminergic vesicles in DA terminals after the Lstim or from DA terminals that were only controlled by Estim but not Lstim. However, the duration of the ARP was prolonged to >4 s by repeated Lstim at 5 Hz (Fig. 4D). When the frequency of Lstim was low, the second pulse of 0.5 Hz Lstim and the third pulse of 1 Hz Lstim still induced DA release (Fig. 4D). These results indicate that the ARP was elongated by high frequency of Lstim, and suggest that cholinergic transmission is responsible for the ARP (Fig. 4D). When the interval between the first Lstim and the Estim increased from 0.05 to 4.1 s, the amplitude of Estim-induced DA release during the ARP increased from 29.5 ± 7.2 to 105.0 ± 1.9 pA (Fig. 4E), and the PPR_{L-E} ($PPR_{L-E} = I_{amp}(Estim)/I_{amp}(Lstim_1)$) also increased from 0.11 ± 0.02 to 0.38 ± 0.04 (Fig. 4E and F), suggesting that this Estim-induced DA release was indeed from a dopaminergic vesicle pool that was undergoing replenishment after partial depletion by the preceding Lstim. Taken together, these results suggest that the ARP of ChI-driven DA release is produced by a cholinergic mechanism, but not by the depletion of dopaminergic vesicles in DA terminals.

We then determined the time course of replenishment of the dopaminergic vesicle pool with paired Lstim–Estim (Fig. 5). As shown above, the increase in $I_{amp}(Estim)$ after the preceding Lstim reflected the DA release from the replenished dopaminergic vesicle pool (Fig. 4E and F). To measure the replenishment of the DA vesicle pool after ChI-driven DA release, we defined the PPR of the DA terminal (PPR_{DT}) as $PPR_{DT} = I_{amp}(Estim, NS)/I_{amp}(Estim_0, NS)$. $I_{amp}(Estim, NS)$ was the nigrostriatal component of $I_{amp}(Estim)$ induced by a test Estim at different intervals (0.05–120 s) following the first Lstim, while the control $I_{amp}(Estim_0, NS)$ was isolated from $I_{amp}(Estim)$ when the DA vesicle pool was intact in resting conditions. $I_{amp}(Estim, NS)$ after Lstim was reduced to 18 ± 3 and $93 \pm 3\%$ of control at the intervals 0.05 and 120 s, respectively

intensity–response dependence of Lstim-induced DA release ($n = 3–7$). Data points are fitted by a Hill function: $y = base + (max - base)/[1 + (x^{half}/x)^{rate}]$, where $base = -0.00796$, $max = 1$, $x^{half} = 1.01$, $rate = 3.53$. G, the latency was in inverse proportion to the amplitude when $I_{amp}(Lstim)$ was obtained at different light intensities ($y = -43.3x + 31.5$, where y is latency in ms, and x is amplitude in pA, $R^2 = 0.957$). H, representative amperometric traces of Lstim-induced DA release recorded at 17, 25 and 32°C in striatal slices. To compare the latencies, all traces were normalized by peak amplitude. I, the latency of Lstim-induced DA release plotted as a function of temperature ($n = 6$ for 17°C, 8 for 25°C and 5 for 32°C).

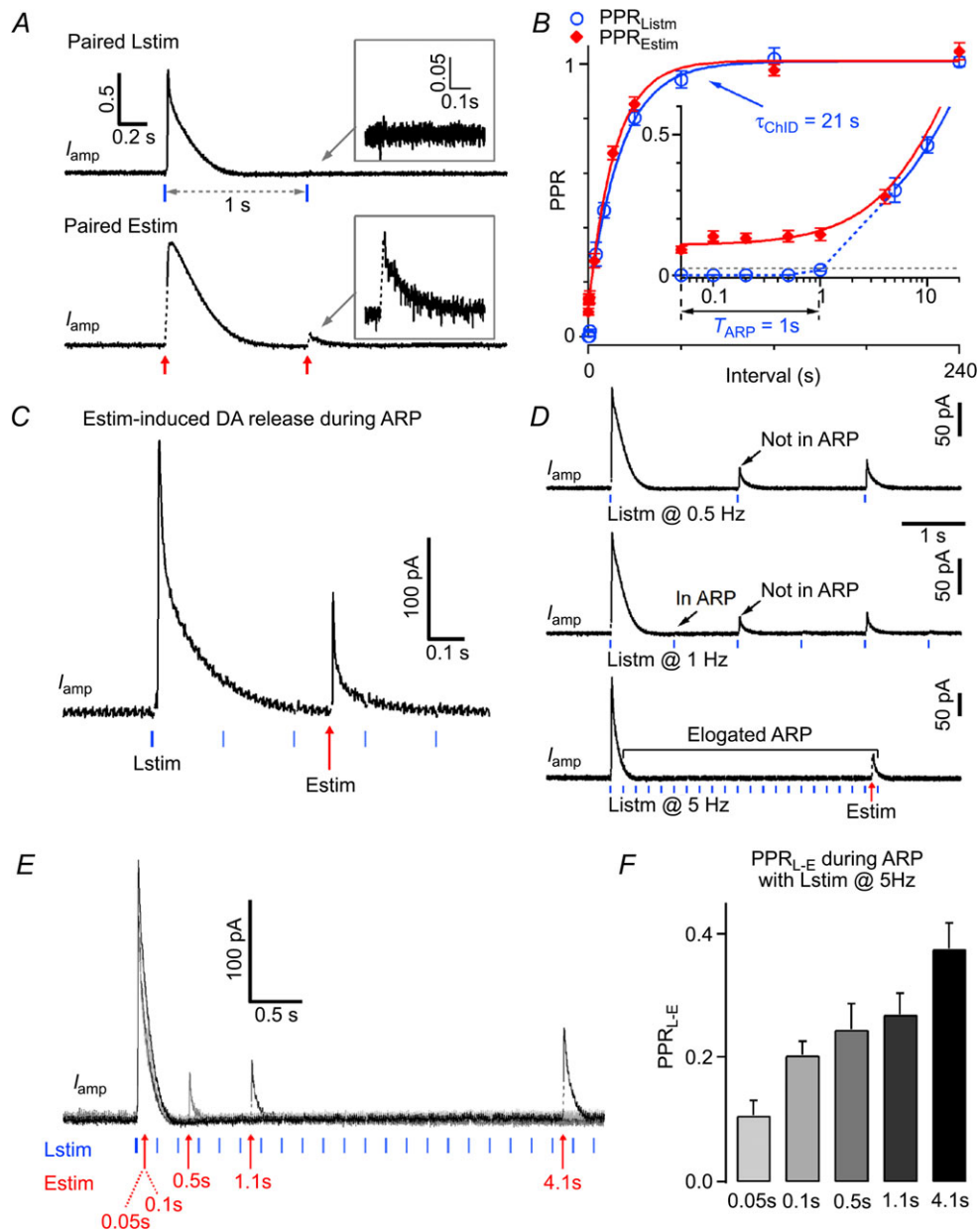


Figure 4. Pared-pulse ratio of dopamine release following optogenetic light stimulation and electrical field stimulation

A, representative normalized I_{amp} traces of DA release induced by paired Lstim (upper) and paired Estim (lower) at a 1 s interpulse interval. Inset, expanded display of I_{amp} by the second pulse. B, PPR recovery time course of DA release after Lstim ($n = 5$) and Estim ($n = 4$). The PPR change within the initial 10 s was magnified (Inset). The PPR of DA release induced by Lstim (PPR_{Lstim}) had two components, a preceding absolute refractory period ($T_{ARP} = 1$ s, when $PPR_{Lstim} < 2\%$), and a subsequent single-exponential recovery ($\tau_{CHID} = 21$ s). Data points of PPR_{Lstim} after 1 s were fitted by a single exponential function: $y = y_0 + Ae^{[-(x-x_0)/\tau]}$, where $y_0 = 1.01$, $A = -0.704$, $x_0 = 5$, $\tau = 20.8$ s. The PPR of DA release induced by Estim (PPR_{Estim}) can be fitted by a constant component (10%) and a single exponential recovery component (90%): $y = y_0 + Ae^{[-(x-x_0)/\tau]}$, where $y_0 = 1.01$, $A = -0.903$, $x_0 = 0.05$, $\tau = 17.1$ s. C, a representative trace showing Estim-induced DA release during the ARP, while the repeated Lstim (the second to the last) failed to induce DA release ($n = 7$). D, representative amperometric traces of DA release induced by repeated Lstim at 0.5 Hz (top, $n = 3$), 1 Hz (middle, $n = 3$) and 5 Hz (bottom, $n = 7$). The duration of the ARP depended on the frequency of the Lstim (ARP < 2 s for 0.5 Hz, 1 s $< ARP < 2$ s for 1 Hz, ARP > 4.2 s for 5 Hz). E, five overlapping recordings as in C, but at different intervals (0.05, 0.1, 0.5, 1.1 and 4.1 s). The Estim during the ARP induced larger DA releases as the interval increased. F, summary of the PPR_{L-E} ($PPR_{L-E} = I_{amp}(Estim)/I_{amp}(Lstim_1)$) at different times during the ARP ($n = 7$).

($PPR_{DT}(0.05\text{ s}) = 18 \pm 3\%$, $PPR_{DT}(120\text{ s}) = 93 \pm 3\%$), indicating that 81% (i.e. $(93\% - 18\%)/93\%$) of $I_{amp}(\text{Estim, NS})$ at the 120 s interval was from replenished dopaminergic vesicles (Fig. 5A). The increase of PPR_{DT} reflected replenishment of the dopaminergic vesicle pool after Lstim-induced depletion. To describe the time course of replenishment, PPR_{DT} data points were fitted by a single exponential function with $\tau_{DT} = 15\text{ s}$ (Fig. 5B).

Together, from the three types of paired stimuli experiments (Lstim–Lstim, Estim–Estim and Lstim–Estim), we determined the time course of dopaminergic vesicle pool replenishment in a single DA terminal ($\tau_{DT} = 15\text{ s}$), as well as the recovery of

the ChI pathway (with refractory time $T_{ARP} = 1\text{ s}$, and replenishment time constant $\tau_{ChID} = 21\text{ s}$) in the complex synapse. We found that replenishment of the dopaminergic vesicle pool *via* the two different pathways had similar time constants ($\tau_{DT} = 15\text{ s}$, $\tau_{ChID} = 21\text{ s}$), while the cholinergic mechanism caused an additional ARP in the recovery of the final ChI-driven DA release.

Discussion

In the present work, by selectively stimulating ChIs and measuring DA release with CFEs, we investigated the

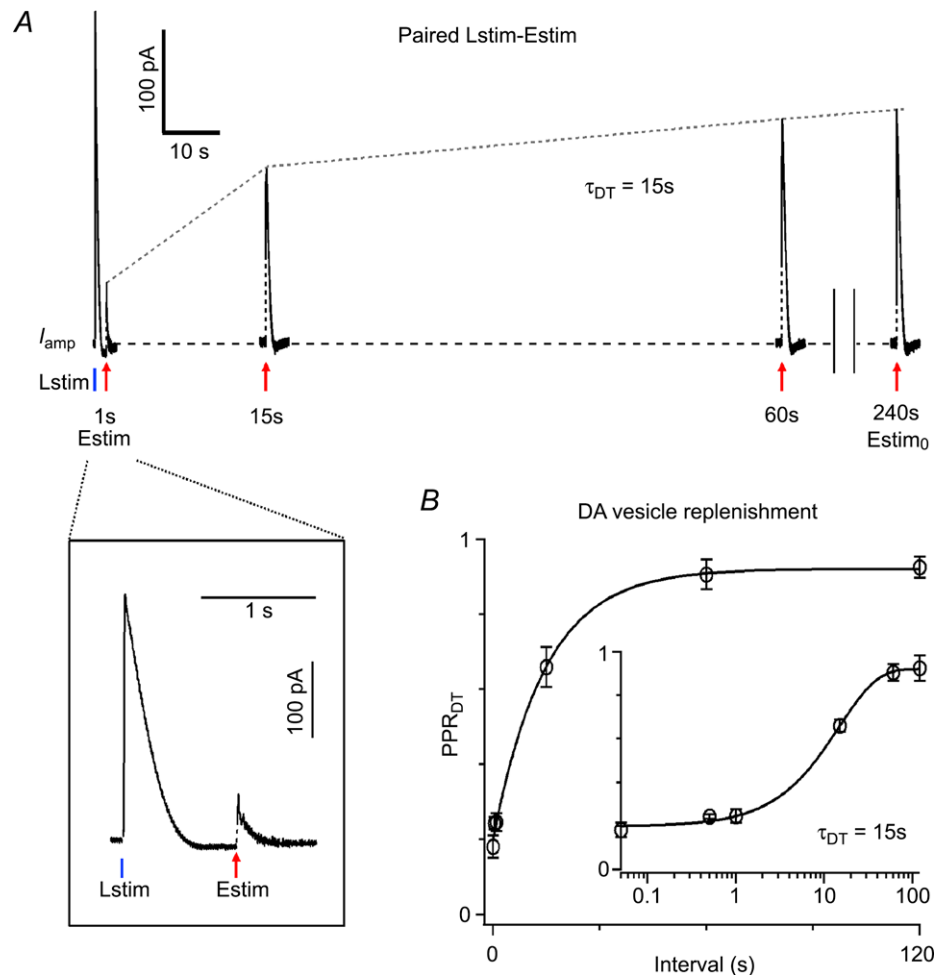


Figure 5. Replenishment of dopaminergic vesicle pool following cholinergic transmission

A, superimposed traces of I_{amp} induced by paired Lstim–Estim with intervals from 1 to 240 s. The control Estim₀ was defined as an Estim with an interval ≥ 4 min. *Inset*, expanded display of I_{amp} induced by paired Lstim–Estim with a 1 s interval. For clarity, the nigrostriatal DA release $I_{amp}(\text{Estim, NS})$ estimated from $I_{amp}(\text{Estim})$ is shown. The percentage replenishment of the dopaminergic vesicle pool was determined by $PPR_{DT} = I_{amp}(\text{Estim, NS})/I_{amp}(\text{Estim}_0, \text{NS})$. B, plot of PPR_{DT} vs. interval (0.05–120 s) between the first $I_{amp}(\text{Lstim})$ and $I_{amp}(\text{Estim, NS})$ ($n = 7$ for 0.5 s point, $n = 8$ for other points). *Inset*, PPR_{DT} was plotted with horizontal log axis to magnify the change of PPR_{DT} within the initial 10 s. Replenishment of the dopaminergic vesicle pool had a single exponential time constant of $\tau_{DT} = 15\text{ s}$. Data points of PPR_{DT} were fitted by a single-exponential function: $y = y_0 + Ae^{\frac{-(x-x_0)}{\tau}}$, where $y_0 = 0.922$, $A = -0.722$, $x_0 = 0.05$, $\tau = 14.7\text{ s}$.

timing of DA release and replenishment through both the nigrostriatal and the ChI pathways in striatal slices. We determined the individual components that contributed to the timing of DA release and replenishment of the dopaminergic vesicle pool for ChI-driven DA release.

Timing of striatal synaptic transmission

One major goal of the present work was to determine the timing of DA release *via* ACh terminal – DA terminal synaptic transmission. Taking advantage of selective optogenetic stimulation, we separated the DA release *via* two different pathways. We measured the latencies of the sequential events in striatal neurotransmission, both within the nigrostriatal pathway and within the ChI pathway, as summarized in Fig. 6A. The latency of DA release *via* the ChI pathway ($t_{\text{aChID}} = 20.6$ ms) was 1.9 times that *via* the nigrostriatal pathway ($t_{\text{aNS}} = 10.8$ ms, Fig. 2D–F).

We estimated the two components of the 17.8 ms ChID latency, the latency of cholinergic transmission (t_{CT} , from cholinergic AP to nAChR activation on the DA terminal) and the latency of dopaminergic transmission (t_{cDT} , from nAChR activation to DA release, ‘cDT’ denotes cholinergic receptor-induced dopaminergic transmission). As indicated in Fig. 6A (a complex synapse may include one or multiple ACh terminals on one DA terminal and part of the axon), cholinergic transmission can trigger a local AP in the DA terminal. In addition to Ca^{2+} influx through nAChRs (Zhou & Neher, 1993), the AP leads to Ca^{2+} influx through voltage-gated Ca^{2+} channels. Under this assumption, the latency of dopaminergic transmission remains the same between the nigrostriatal ($t_{\text{aNS}} = t_{\text{dAP}} + t_{\text{NS}} = 10.8$ ms) and ChI pathways ($t_{\text{cDT}} = t_{\text{aNS}} = t_{\text{dAP}} + t_{\text{NS}} = 10.8$ ms), and the latency of the corresponding cholinergic transmission is $t_{\text{CT}} = t_{\text{ChID}} - t_{\text{cDT}} = 7.0$ ms, where 1.9 ms (t_{dAP}) is for the AP firing in the DA neuron and 2.8 ms (t_{cAP}) is for the AP firing in the ChI, assuming the same latency for the somatic and terminal APs. Alternatively, if a local AP is not generated in the DA terminal during ChI-driven DA release, and Ca^{2+} influx occurs only through the nAChRs, the latency of dopaminergic transmission is $t_{\text{cDT}} = t_{\text{NS}} = t_{\text{aNS}} - t_{\text{dAP}} = 8.9$ ms, and the latency of the corresponding cholinergic transmission would be $t_{\text{CT}} = t_{\text{ChID}} - t_{\text{cDT}} = 8.9$ ms, which is 1.9 ms longer than t_{CT} proposed in Fig. 6A. Since the latency of cholinergic transmission (t_{CT}) was only 7–9 ms at room temperature, which is quite close to glutamate synaptic transmission (1–5 ms; Sabatini & Regehr, 1996; Huang *et al.* 2007). Regarding previous anatomical works on cholinergic synaptic structures in the dorsal striatum, the present physiological finding is consistent with some observations (Wainer *et al.* 1984; Phelps *et al.* 1985) but

not others (Descarries *et al.* 1997; Descarries & Mechawar, 2000). Future work should determine whether synaptic or asynaptic cholinergic transmission is responsible for ChI-driven DA release.

The total latency of ChI-driven DA release (t_{aChID}) could be regulated by presynaptic vesicular ACh release. After inhibition of VAcHT with vesamicol, the Lstim-induced DA release was completely blocked and the latency of $I_{\text{amp}}(\text{Lstim})$ was prolonged (Fig. 3A–D). Vesamicol also totally blocked the phase II component of $I_{\text{amp}}(\text{Estim})$ (data not shown), which is consistent with its effect on the Lstim-induced DA release. Vesamicol reduced the amplitude of the phase I component of $I_{\text{amp}}(\text{Estim})$ by ~30%, which might be an indirect effect (data not shown). Thus, presynaptic vesicular release not only influenced the strength of the postsynaptic response but also regulated the latency of DA release *via* the terminal–terminal connection.

Considering that the expression level of VAcHT is enhanced in ChAT-ChR2-EYFP transgenic mice (Kolisnyk *et al.* 2013), we recorded the Estim-induced DA release in wild-type C57BL/6 mice. A biphasic onset of $I_{\text{amp}}(\text{Estim})$ was also found in these mice (Fig. 2G). The latency of DA release *via* the two pathways, which can be estimated by the latency of the two phases of $I_{\text{amp}}(\text{Estim})$, showed no significant difference between wild-type and transgenic mice (Fig. 2H). These results suggest that the over-expression of VAcHT in ChAT-ChR2-EYFP mice does not affect the timing of DA release in striatal brain slices, although some behaviours of the transgenic mice are changed (Kolisnyk *et al.* 2013). Note that, considering Estim-induced artifacts were right before I_{amp} signal (Methods), 10.8 ms is upper limit of phase-I latency (Figs. 2 and 6).

We measured DA release by amperometry and FCV. Transient increases in local DA concentration $[\text{DA}]_e$ (or ‘DA overflow’) from DA release can be detected by both FCV and amperometry (Wightman, 2006; Wang *et al.* 2011). $[\text{DA}]_e$ recorded by FCV mimics the real profile of native $[\text{DA}]_e$, because DA molecules are first oxidized and then reduced by the CFE at a changing voltage during a cyclical voltage scanning period. In contrast, amperometry detects $[\text{DA}]_e$ at a constant voltage (Wightman *et al.* 1991; Chow *et al.* 1992; Zhou & Misler, 1995). Therefore, amperometry has a temporal resolution >100-fold higher than FCV (0.5 vs. 100 ms) in $[\text{DA}]_e$ recording. This greater time resolution is key to determining the temporal components during synaptic transmission in brain slices at the millisecond level (Figs 1 and 2; see also Bruns & Jahn, 1995; Wightman, 2006; Huang *et al.* 2007).

Timing of vesicle pool replenishment

Our second major finding was the time courses of the components of DA vesicle replenishment in the

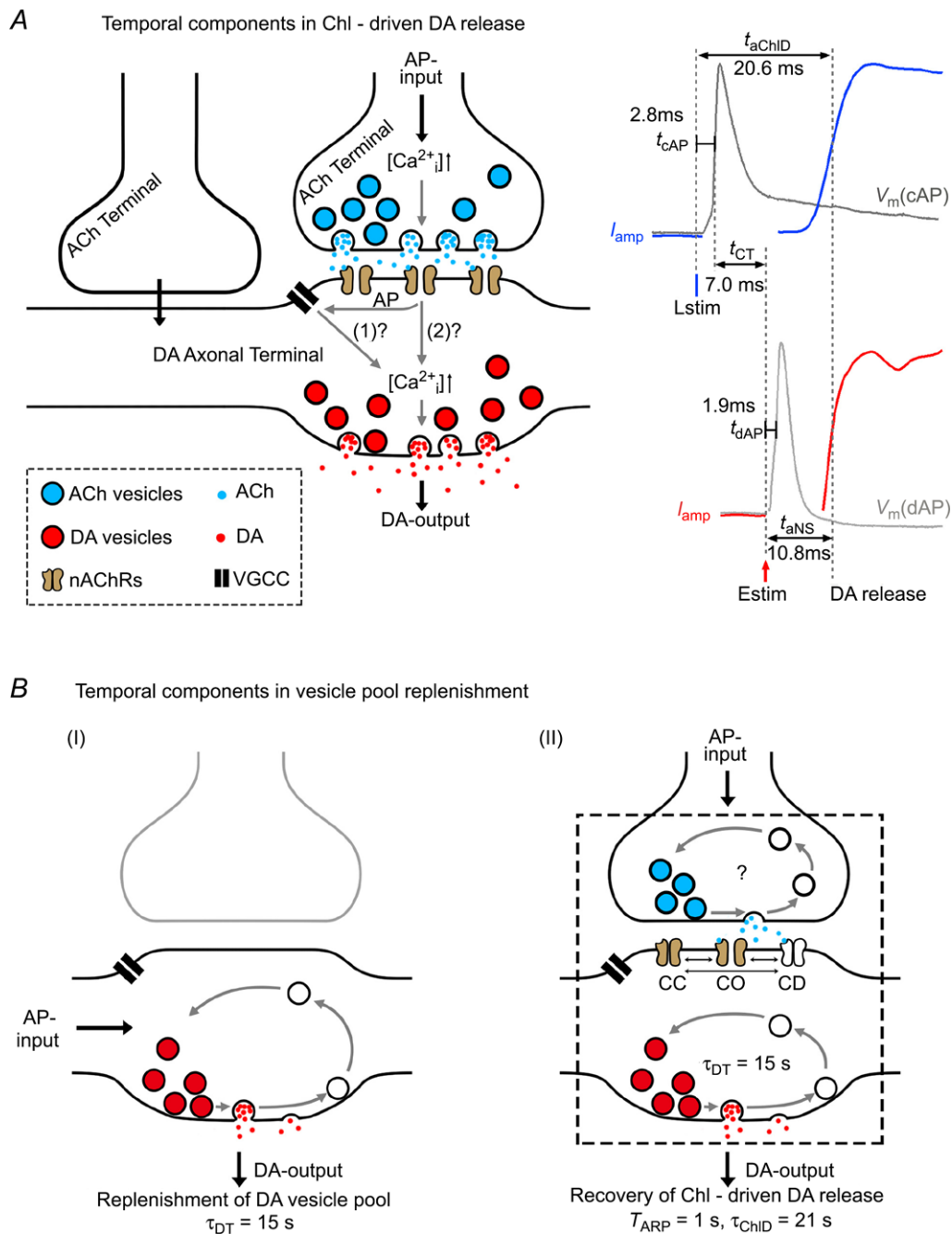


Figure 6. Model of DA release via the cholinergic interneuron pathway in the striatum

A, temporal components in DA release via the Chl pathway. Lstim selectively activates ChR2, elicits action potential (AP) firing in Chls within 2.8 ± 0.1 ms (t_{cAP}) and induces cholinergic synaptic transmission ($t_{CT} = 7.0 \pm 0.4$ ms). Following the synchronized ACh release from multiple ACh terminals (Threlfell *et al.* 2012), the local postsynaptic nAChRs on DA terminals (local axons) are activated, leading to Ca^{2+} influx into the DA terminal either through activating a dopaminergic AP ($t_{dAP} = 1.9 \pm 0.2$ ms) and voltage-gated Ca^{2+} channels or directly through the nAChRs. The increased $[Ca^{2+}]_i$ triggers DA release (DA-output) and finishes dopaminergic transmission (estimated from I_{amp} (Estim, NS), $t_{aNS} = 10.8 \pm 0.2$ ms) as well as Chl-driven DA release ($t_{CHID} = 17.8 \pm 0.3$ ms). Total Lstim-induced DA release takes time $t_{aCHID} = t_{cAP} + t_{CHID}$, while Estim-induced DA release takes time t_{aNS} . **B**, temporal components in vesicle pool replenishment after Chl-driven DA release. *I*, for a DA terminal, with AP input and DA output, the PPR recovery follows the classical law (eqn (3)) with a single exponential time constant of $\tau_{DT} = 15$ s. *II*, for a complex terminal-terminal synapse, the PPR recovery follows a non-classical format (eqn (1)), with a preceding 1 s absolute refractory period ($T_{ARP} = 1$ s) and a subsequent classical time constant of $\tau_{CHID} = 21$ s. CC, nAChR channel closed; CO, channel open; CD, channel desensitized.

nigrostriatal and ChI pathways. Threlfell *et al.* (2012) have shown that the DA release evoked by a single light flash (and APs in ChIs) is unresponsive to subsequent light flashes in short trains of APs lasting 10–1000 ms. We extended this and found that $I_{\text{amp}}(\text{Lstim})$ had an ARP, which was 1000 ms, because after 1000 ms the ChI-driven DA release started to recover with a time constant of 21 s (Fig. 4B). Threlfell *et al.* (2012) identified that this refractory mechanism does not occur for DA release driven directly from DA axons by activity in DA neurons. In the present work, we further found that the ARP was prolonged from 1 to >4 s by 5 Hz Lstim but not by 0.5 or 1 Hz Lstim. Because the frequency could only affect cholinergic transmission, the ARP elongation suggests that cholinergic transmission is responsible for the ARP (Figs 4D and 6). The elongation further implicates that Lstim-induced ACh release exists even during ARP. During the ARP, the amplitude of $I_{\text{amp}}(\text{Estim})$ increased as the interval increased (Fig. 4E and F), confirming that Estim-induced DA release during the ARP was indeed from a dopaminergic vesicle pool that was being replenished after partial depletion by the preceding Lstim. These findings suggest a simple hypothesis for the refractory mechanism: for a short period after the first successful ChI-driven DA release, the cholinergic transmission is decreased to a sub-threshold level such that the intra-terminal Ca^{2+} is unable to release DA, even though the dopaminergic vesicle pool is still available.

The existence of the ARP suggests that the complex synapse (terminal–terminal structure) as a whole does not follow the classical law of vesicle pool replenishment for the single-terminal synapse (eqn (3)). Instead, the ARP follows a theoretical prediction that the complex type III synapse has two replenishment components ($I_{\text{ChID}} = 0$, ($t \leq T_{\text{ARP}}$); $I_{\text{ChID}} = 1 - e^{-\frac{t}{\tau_{\text{ChID}}}}$ ($t > T_{\text{ARP}}$); see eqn (1)). Within the ARP, the vesicles in DA terminals probably ‘see’ only sub-threshold Ca^{2+} signals following the second Lstim of paired Lstim–Lstim. Alternatively, the ARP could also be due to desensitization of nAChRs and/or temporal modifications of the vesicle-fusion machinery.

In the ChI pathway, the cholinergic terminal in eqn (1) is the presynaptic component, while the DA terminal is the postsynaptic component. Although the complex synapse as a whole did not follow the classical law of the single-terminal synapse (eqn (3)), the DA terminal itself did follow this law. When the DA terminal was examined in terms of the PPR made by paired Lstim–Estim (Fig. 5), the vesicle pool replenishment had a single classical component ($\tau_{\text{DT}} = 15$ s). Immediately after the first non-classical replenishment component ARP ($T_{\text{ARP}} = 1$ s), the second replenishment component of ChI-driven DA release fitted the classical law (eqn (3)) for single-vesicle pool replenishment ($\tau_{\text{ChID}} = 21$ s, see Fig. 4B). According to eqn (1), after the ARP, the recovery time constant of the

ChI-driven DA release would be determined by the DA terminal, $S(t) = S_b(t)$, or $\tau_{\text{ChID}} = \tau_{\text{DT}}$. In fact, the τ_{ChID} (21 s) was slightly slower but close to τ_{DT} (15 s).

Thus, the replenishment of the DA terminal has a single classical component (τ_{DT}), while the replenishment of the ‘complex terminal’ has a non-classical component (T_{ARP}) followed by a classical component (τ_{ChID} , Fig. 6B). Note that although here we used the hypothesis of vesicle pool replenishment to quantitatively interpret our PPR data about recovery of transmitter release, the recovery of release can also be due to mechanisms other than replenishment of the pool.

Physiological relevance of synaptic terminal–terminal transmission

In the striatum, to conduct DA-dependent behavioural tasks under physiological conditions, DA release can be triggered by any of three modes: (i) the ascending pathway *via* the nigrostriatal projection, (ii) the ChI pathway *via* cholinergic terminal–dopaminergic terminal transmission, or (iii) both pathways. Different modes of DA release may act differently in behavioural tasks. The timing of DA release may produce behavioural outputs such as cocaine self-administration (a latency of 1–3 s for DA release preceding action (Phillips *et al.* 2003)) and food seeking (a latency of 0.2 s for DA release preceding action (Roitman *et al.* 2004)).

Temporally precise DA neuronal signalling codes reward prediction error, and drives reward-related learning (Schultz *et al.* 1997; Steinberg *et al.* 2013). The control of corticostriatal synaptic plasticity is thought to be an important mechanism underlying this process (Reynolds *et al.* 2001; Surmeier *et al.* 2007). Furthermore, it is well known that the critical time window to form LTP or LTD is about ± 50 ms (Caporale & Dan, 2008). The timing of presynaptic and postsynaptic firing determines the direction of the synaptic plasticity (spike-timing-dependent plasticity, STDP) (Markram *et al.* 1997; Caporale & Dan, 2008). For example, post-synaptic firing with a 10 ms delay after presynaptic firing ($\Delta t = 10$ ms) normally induces LTP, whereas the reverse order of firing ($\Delta t = -10$ ms) induces LTD. In many brain regions, including the striatum, DA controls the induction of STDP and even reverses it (i.e. LTP at $\Delta t = -10$ ms) (Pawlak & Kerr, 2008; Shen *et al.* 2008; Zhang *et al.* 2009), implying that precise DA signalling is essential for determining synaptic plasticity, and for learning and memory. In the present work, we demonstrated that the temporal components within a single case of DA synaptic transmission are ~ 10 or ~ 20 ms, both of which are within the critical time window. Although the exact temporal relationship between the DA signal and

LTP/LTD formation is unclear, the temporal components of synaptic transmission *via* both the nigrostriatal and the ChI pathways will be helpful to reveal the relationship in future studies.

This work was mainly carried out at room temperature. The transmitter release and vesicle pool replenishment would be faster at physiological temperature (Sabatini & Regehr, 1996). Therefore, we studied the correlation of the latency of ChI-driven DA release *vs.* temperature. The latency of I_{amp} (Lstim) was reduced as the temperature was increased, suggesting that the ChI-driven DA release is faster at a near-physiological temperature than at room temperature (Fig. 3H and I).

We have discovered distinct timing features for both release latency and replenishment of the ChI pathway, which may impact DA-dependent circuits and thus be relevant to DA-related behaviours such as smoke seeking.

References

- Arbuthnott GW & Wickens J (2007). Space, time and dopamine. *Trends Neurosci* **30**, 62–69.
- Augustine G, Charlton M & Smith S (1985). Calcium entry and transmitter release at voltage-clamped nerve terminals of squid. *J Physiol* **367**, 163–181.
- Augustine GJ, Charlton MP & Smith SJ (1987). Calcium action in synaptic transmitter release. *Ann Rev Neurosci* **10**, 633–693.
- Betz WJ (1970). Depression of transmitter release at the neuromuscular junction of the frog. *J Physiol* **206**, 629–644.
- Boyden ES, Zhang F, Bamberg E, Nagel G & Deisseroth K (2005). Millisecond-timescale, genetically targeted optical control of neural activity. *Nat Neurosci* **8**, 1263–1268.
- Bruns D & Jahn R (1995). Real-time measurement of transmitter release from single synaptic vesicles. *Nature* **377**, 62–65.
- Cachope R, Mateo Y, Mathur BN, Irving J, Wang HL, Morales M, Lovinger DM & Cheer JF (2012). Selective activation of cholinergic interneurons enhances accumbal phasic dopamine release: setting the tone for reward processing. *Cell Rep* **2**, 33–41.
- Caporale N & Dan Y (2008). Spike timing-dependent plasticity: a Hebbian learning rule. *Ann Rev Neurosci* **31**, 25–46.
- Chen XK, Wang LC, Zhou Y, Cai Q, Prakriya M, Duan KL, Sheng ZH, Lingle C & Zhou Z (2005). Activation of GPCRs modulates quantal size in chromaffin cells through $G_{\beta\gamma}$ and PKC. *Nat Neurosci* **8**, 1160–1168.
- Chow RH, von Ruden L & Neher E (1992). Delay in vesicle fusion revealed by electrochemical monitoring of single secretory events in adrenal chromaffin cells. *Nature* **356**, 60–63.
- Cragg SJ (2003). Variable dopamine release probability and short-term plasticity between functional domains of the primate striatum. *J Neurosci* **23**, 4378–4385.
- Dan Y & Poo MM (2006). Spike timing-dependent plasticity: from synapse to perception. *Physiol Rev* **86**, 1033–1048.
- Dani JA & Bertrand D (2007). Nicotinic acetylcholine receptors and nicotinic cholinergic mechanisms of the central nervous system. *Ann Rev Pharmacol Toxicol* **47**, 699–729.
- Descarries L, Gisiger V & Steriade M (1997). Diffuse transmission by acetylcholine in the CNS. *Prog Neurobiol* **53**, 603–625.
- Descarries L & Mechawar N (2000). Ultrastructural evidence for diffuse transmission by monoamine and acetylcholine neurons of the central nervous system. *Prog Brain Res* **125**, 27–47.
- Dittman JS & Regehr WG (1998). Calcium dependence and recovery kinetics of presynaptic depression at the climbing fibre to Purkinje cell synapse. *J Neurosci* **18**, 6147–6162.
- Elmqvist D & Quastel DM (1965). A quantitative study of end-plate potentials in isolated human muscle. *J Physiol* **178**, 505–529.
- Enomoto K (1988). Post- and presynaptic effects of vesamicol (AH5183) on the frog neuromuscular junction. *Eur J Pharmacol* **147**, 209–215.
- Huang HP, Wang SR, Yao W, Zhang C, Zhou Y, Chen XW, Zhang B, Xiong W, Wang LY, Zheng LH, Landry M, Hokfelt T, Xu ZQ & Zhou Z (2007). Long latency of evoked quantal transmitter release from somata of locus coeruleus neurons in rat pontine slices. *Proc Natl Acad Sci U S A* **104**, 1401–1406.
- Kandel ER, Schwartz JH & Jessell TM (2000). *Principles of Neural Science*, Vol. 4. McGraw-Hill, New York.
- Katz B (1969). *The Release of Neural Transmitter Substances*. Liverpool University Press, Liverpool.
- Katz B & Miledi R (1965). The measurement of synaptic delay, and the time course of acetylcholine release at the neuromuscular junction. *Proc R Soc Lond B Biol Sci* **161**, 483–495.
- Kolisnyk B, Guzman MS, Raulic S, Fan J, Magalhaes AC, Feng G, Gros R, Prado VF & Prado MA (2013). ChAT-ChR2-EYFP mice have enhanced motor endurance but show deficits in attention and several additional cognitive domains. *J Neurosci* **33**, 10427–10438.
- Kusano K & Landau EM (1975). Depression and recovery of transmission at the squid giant synapse. *J Physiol* **245**, 13–32.
- Liu T, Shang SJ, Liu B, Wang CH, Wang YS, Xiong W, Zheng LH, Zhang CX & Zhou Z (2011). Two distinct vesicle pools for depolarization-induced exocytosis in somata of dorsal root ganglion neurons. *J Physiol* **589**, 3507–3515.
- Lupa MT (1988). Effects of an inhibitor of the synaptic vesicle acetylcholine transport system on quantal neurotransmitter release: an electrophysiological study. *Brain Res* **461**, 118–126.
- Markram H, Lubke J, Frotscher M & Sakmann B (1997). Regulation of synaptic efficacy by coincidence of postsynaptic APs and EPSPs. *Science* **275**, 213–215.
- Neher E & Sakaba T (2008). Multiple roles of calcium ions in the regulation of neurotransmitter release. *Neuron* **59**, 861–872.
- Nicola SM, Surmeier J & Malenka RC (2000). Dopaminergic modulation of neuronal excitability in the striatum and nucleus accumbens. *Ann Rev Neurosci* **23**, 185–215.

- Otsuka M, Endo M & Nonomura Y (1962). Presynaptic nature of neuromuscular depression. *Jpn J Physiol* **12**, 573–584.
- Pan B & Zucker RS (2009). A general model of synaptic transmission and short-term plasticity. *Neuron* **62**, 539–554.
- Pawlak V & Kerr JN (2008). Dopamine receptor activation is required for corticostriatal spike-timing-dependent plasticity. *J Neurosci* **28**, 2435–2446.
- Phelps PE, Houser CR & Vaughn JE (1985). Immunocytochemical localization of choline acetyltransferase within the rat neostriatum: a correlated light and electron microscopic study of cholinergic neurons and synapses. *J Comp Neurol* **238**, 286–307.
- Phillips PE, Stuber GD, Heien ML, Wightman RM & Carelli RM (2003). Subsecond dopamine release promotes cocaine seeking. *Nature* **422**, 614–618.
- Ren J, Qin C, Hu F, Tan J, Qiu L, Zhao S, Feng G & Luo M (2011). Habenula ‘cholinergic’ neurons co-release glutamate and acetylcholine and activate postsynaptic neurons via distinct transmission modes. *Neuron* **69**, 445–452.
- Reynolds JN, Hyland BI & Wickens JR (2001). A cellular mechanism of reward-related learning. *Nature* **413**, 67–70.
- Rice ME & Cragg SJ (2004). Nicotine amplifies reward-related dopamine signals in striatum. *Nat Neurosci* **7**, 583–584.
- Rizzoli SO & Betz WJ (2005). Synaptic vesicle pools. *Nat Rev Neurosci* **6**, 57–69.
- Roitman MF, Stuber GD, Phillips PE, Wightman RM & Carelli RM (2004). Dopamine operates as a subsecond modulator of food seeking. *J Neurosci* **24**, 1265–1271.
- Sabatini BL & Regehr WG (1996). Timing of neurotransmission at fast synapses in the mammalian brain. *Nature* **384**, 170–172.
- Sabatini BL & Regehr WG (1999). Timing of synaptic transmission. *Ann Rev Physiol* **61**, 521–542.
- Schmitz Y, Schmauss C & Sulzer D (2002). Altered dopamine release and uptake kinetics in mice lacking D2 receptors. *J Neurosci* **22**, 8002–8009.
- Schultz W (2007). Multiple dopamine functions at different time courses. *Ann Rev Neurosci* **30**, 259–288.
- Schultz W, Dayan P & Montague PR (1997). A neural substrate of prediction and reward. *Science* **275**, 1593–1599.
- Shen W, Flajolet M, Greengard P & Surmeier DJ (2008). Dichotomous dopaminergic control of striatal synaptic plasticity. *Science* **321**, 848–851.
- Sorensen JB, Nagy G, Varoqueaux F, Nehring RB, Brose N, Wilson MC & Neher E (2003). Differential control of the releasable vesicle pools by SNAP-25 splice variants and SNAP-23. *Cell* **114**, 75–86.
- Steinberg EE, Keiflin R, Boivin JR, Witten IB, Deisseroth K & Janak PH (2013). A causal link between prediction errors, dopamine neurons and learning. *Nat Neurosci* **16**, 966–973.
- Sudhof TC (2004). The synaptic vesicle cycle. *Ann Rev Neurosci* **27**, 509–547.
- Surmeier DJ, Ding J, Day M, Wang Z & Shen W (2007). D1 and D2 dopamine-receptor modulation of striatal glutamatergic signalling in striatal medium spiny neurons. *Trends Neurosci* **30**, 228–235.
- Threlfell S, Lalic T, Platt NJ, Jennings KA, Deisseroth K & Cragg SJ (2012). Striatal dopamine release is triggered by synchronized activity in cholinergic interneurons. *Neuron* **75**, 58–64.
- Wainer BH, Bolam JP, Freund TF, Henderson Z, Totterdell S & Smith AD (1984). Cholinergic synapses in the rat brain: a correlated light and electron microscopic immunohistochemical study employing a monoclonal antibody against choline acetyltransferase. *Brain Res* **308**, 69–76.
- Wang L, Shang SJ, Zheng LH & Zhou Z (2013). Temporal components of a synaptic terminal-terminal transmission in dorsal striatum slices. In *Neuroscience 2013*. Society for Neuroscience, San Diego, CA.
- Wang SR, Yao W, Huang HP, Zhang B, Zuo PL, Sun L, Dou HQ, Li Q, Kang XJ, Xu HD, Hu MQ, Jin M, Zhang L, Mu Y, Peng JY, Zhang CX, Ding JP, Li BM & Zhou Z (2011). Role of vesicle pools in action potential pattern-dependent dopamine overflow in rat striatum *in vivo*. *J Neurochem* **119**, 342–353.
- Wightman RM (2006). Detection technologies. Probing cellular chemistry in biological systems with microelectrodes. *Science* **311**, 1570–1574.
- Wightman RM, Jankowski JA, Kennedy RT, Kawagoe KT, Schroeder TJ, Leszczyszyn DJ, Near JA, Diliberto EJ, Jr & Viveros OH (1991). Temporally resolved catecholamine spikes correspond to single vesicle release from individual chromaffin cells. *Proc Natl Acad Sci U S A* **88**, 10754–10758.
- Wu LG (2004). Kinetic regulation of vesicle endocytosis at synapses. *Trends Neurosci* **27**, 548–554.
- Zhang B, Sun L, Yang YM, Huang HP, Zhu FP, Wang L, Zhang XY, Guo S, Zuo PL, Zhang CX, Ding JP, Wang LY & Zhou Z (2011). Action potential bursts enhance transmitter release at a giant central synapse. *J Physiol* **589**, 2213–2227.
- Zhang B, Zhang XY, Luo PF, Huang W, Zhu FP, Liu T, Du YR, Wu QH, Lu J, Xiu Y, Liu LN, Huang HP, Guo S, Zheng H, Zhang CX & Zhou Z (2012). Action potential-triggered somatic exocytosis in mesencephalic trigeminal nucleus neurons in rat brain slices. *J Physiol* **590**, 753–762.
- Zhang H & Sulzer D (2004). Frequency-dependent modulation of dopamine release by nicotine. *Nat Neurosci* **7**, 581–582.
- Zhang JC, Lau PM & Bi GQ (2009). Gain in sensitivity and loss in temporal contrast of STDP by dopaminergic modulation at hippocampal synapses. *Proc Natl Acad Sci U S A* **106**, 13028–13033.
- Zhao S, Ting JT, Atallah HE, Qiu L, Tan J, Gloss B, Augustine GJ, Deisseroth K, Luo M, Graybiel AM & Feng G (2011). Cell type-specific channelrhodopsin-2 transgenic mice for optogenetic dissection of neural circuitry function. *Nat Methods* **8**, 745–752.
- Zhou FM, Liang Y & Dani JA (2001). Endogenous nicotinic cholinergic activity regulates dopamine release in the striatum. *Nat Neurosci* **4**, 1224–1229.
- Zhou Z & Mislis S (1995). Action potential-induced quantal secretion of catecholamines from rat adrenal chromaffin cells. *J Biol Chem* **270**, 3498–3505.
- Zhou Z & Neher E (1993). Calcium permeability of nicotinic acetylcholine receptor channels in bovine adrenal chromaffin cells. *Pflugers Arch* **425**, 511–517.

Additional information

Competing interests

The authors declare no competing interests.

Author contributions

L.W., X.Z., H.X., L.Z., R.J., W.L., F.Z., X.K., B.L., S.T., Q.W., M.L., H.D., P.Z., C.W. and S.W. carried out the experiments. Z.Z. and L.W. planned the work and wrote the paper.

Funding

This work was supported by grants from the National Basic Research Program of China (2012CB518006), the National Natural Science Foundation of China (31228010, 31171026, 31100597, 31327901, 31221002 and 31330024), the National Key Technology R&D Program (SQ2011SF11B01041) and a '985' grant from the Department of Education of China.

Acknowledgements

We thank Drs Guoping Feng and Minmin Luo for providing ChAT-ChR2-EYFP mice and help, and Drs Luyang Wang and Iain C. Bruce for comments on the manuscript.